Optics & Laser Technology 161 (2023) 109171

Contents lists available at ScienceDirect

Optics and Laser Technology

journal homepage: www.elsevier.com/locate/optlastec

Full length article

Highly sensitive detection of trace lead ions concentration based on a functional film-enhanced optical microfiber sensor

Guoquan Wang [a], Dandan Sun [a,*], Lili Liang [b], Guanjun Wang [c], Jie Ma [a,d]

[a] School of Physics and Electronic Engineering, Shanxi University, Taiyuan, China
[b] Hebei Key Laboratory of Optical Fiber Biosensing and Communication Devices, Institute of Information Technology, Handan University, Handan 056005, China
[c] School of Information and Communication Engineering, Hainan University, Haikou 570228, China
[d] Collaborative Innovation Center of Extreme Optics, Shanxi University, Taiyuan, China

ARTICLE INFO

Keywords:
Lead ions
Microfiber interferometer
Optical microfiber pollutant sensor
Functional Film

ABSTRACT

An optical fiber sensor for detecting the concentration of trace lead ions is proposed using a polydopamine-maleic acid (PDA-MA) functional membrane coated on the surface of a Mach-Zehnder microfiber interferometer. The PDA-MA functional film is wrapped by a one-step immersion method for in-situ growth on the interferometer surface. The microfiber surface has an excellent evanescent field possessing a sensitivity to the ambient RI of 1243.455 nm/RIU and a low temperature cross-reactivity of −0.04 nm/°C. The absorption of lead ions by carboxyl groups in the fiber-coated functional film changes the refractive index of the sensor surface, which reflects a macroscopic wavelength shift in the interference spectrum. The sensor effectively detects lead ions within 10^{-14}-10^{-6} mol/L concentrations and has a sensitivity of 1.85×10^{8} nm/(mol/L) in the ultra-low concentration range of 10^{-14}-10^{-10} mol/L with a detection limit of 0.1678 ppb. The proposed sensor is not only simple and low cost to fabricate, but also has good stability and specificity. The success of this sensor shows that the development of optical microfiber sensor with high stability and accuracy is feasible, which has progressive significance for the research of optical environmental pollution sensor.

1. Introduction

Environmental pollution has become a major threat at the global level because of the long-term harm to ecosystems and consequently the direct health hazards to humans. Among environmental pollution, the problem of pollution in the aquatic domain is particularly obvious. Various pollutants such as cresols, creatinine and heavy metal ions can cause serious damage to human functions if absorbed into the body. Phenolic compounds easily releasing toxic gases, if inhaled, can be harmful to human health, and drinking water containing high concentrations of p-cresol can cause some muscle twitch, difficulty walk, and even death [1]. Creatinine, on the other hand, is an important clinical biomarker for major diseases such as diabetes and kidney disease [2]. The contamination of heavy metal ions and their harmful effects on the human body are equally severe. As the accelerated global urbanization and industrialization, the pollution of heavy metal ions is ubiquitous, toxic and non-biodegradable, which affecting the quality of different soils and aquatic organisms [3]. More particularly, heavy metal ions such as lead, sodium, cadmium, mercury and copper are easily dissolved in water and enter the biosphere without decomposition, even they accumulate in living organisms with serious consequence. Therefore, heavy metal ions in water are considered to be extremely hazardous to human health and ecosystems [4].

Among heavy metal contaminants, lead ions (Pb^{2+}) are one of the most common pollutants, which ranking second in the list of toxic substances [5]. With the advantages of low melting point, high corrosion resistance and good plasticity, lead is extensively used in industrial production and daily life. However, due to the adsorption of soil colloids and particulate matter, lead ions leak into the soil and will exist in the soil for a long time, and heavy metals cannot be degraded by microorganisms, which is a long-term and potential pollutant in the environment [6]. It is well known that Pb^{2+} tends to accumulate rather than decompose, and when ingested in excess Pb^{2+} lead to nervous system diseases, including headache, irritability, lethargy, convulsions, muscle weakness, ataxia, tremor, paralysis and so on, even exposure to or ingestion of trace amounts of Pb^{2+} can cause serious damage to the kidney, brain and other organs [7].

Several organizations, including the World Health Organization

* Corresponding author.
E-mail addresses: sundd@sxu.edu.cn, mj@sxu.edu.cn (D. Sun).

https://doi.org/10.1016/j.optlastec.2023.109171
Received 10 November 2022; Received in revised form 27 December 2022; Accepted 9 January 2023
Available online 28 January 2023

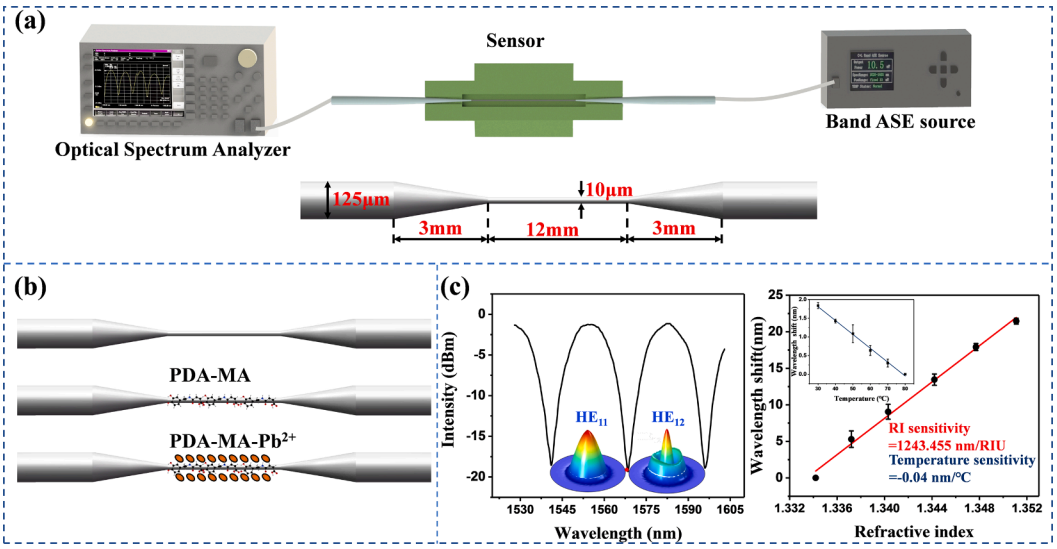

Fig. 1. (a) The diagram of microfiber sensor detection system and the microfiber interferometer structure with parameters; (b) The schematic diagram of Pb^{2+} concentration detection by PDA-MA film functionalized microfiber sensor; (c) The interferential spectrum of the microfiber interferometer, the insets are the transverse electric field amplitude distribution of HE_{11} and HE_{12} in the major interference modes (left); RI and temperature response of the microfiber interferometer with error bar (right).

(WHO), the International Agency for Research on Cancer, the Food and Agriculture Organization, and the Centers for Disease Control, have listed Pb^{2+} as a carcinogen requiring to be monitored. The WHO has set the allowable concentration of lead ions in drinking water to no more than 10 ppb according to environmental quality standards [5].

In the past research studies, researchers have carried out various methods to determine the Pb^{2+} concentration in aqueous solution, including atomic absorption spectrometry analysis [8], fluorescence analysis [9], electrochemical analysis [10] and X-ray fluorescence spectrometry [11]. These methods can effectively detect the Pb^{2+} concentration in aqueous solutions with high accuracy. However, their pretreatment requirements are high, the detection costs are high, and some of them may produce toxic by-products [12]. For example, atomic absorption spectrometry analysis method requires a lot of chemical reagents such as sodium diethyldithiocarbamate [8], which can easily cause environmental pollution and physical illness. Therefore, it is of great significance and tremendous challenges simultaneously to develop a simple and effective method to determine the Pb^{2+} concentration in water environment.

Optical fiber sensor, due to their low cost, light weight, small size, resistance to electromagnetic interference, high sensitivity, corrosion resistance, and easy implementation of multiplexed or distributed remote sensing, has been increasingly investigated as a potential sensing tool [13,14]. At present, optical fiber sensors have been widely used in many types of monitoring, such as temperature [15], strain, environment [16], biological sensing [17–19] and heavy metal detection [20].

Various lead ion sensors with different optical fiber structures have been reported. Jenny et al. (2010) have made a lead ion sensor with periodic mesoporous organosilica coated long period fiber grating [21]. Liu et al. (2018) have proposed a tilted fiber grating immobilized black phosphorus for trace detection of Pb^{2+} [22]. Yap et al. (2018) have achieved the measurement of Pb^{2+} concentration in the 5–50 μg/L range by using a tapered microfiber sensor coated with L-glutathione [23]. Yin et al. (2019) have developed a microfiber coil resonator based on black phosphorus to detect Pb^{2+} in water [7]. Noman et al. (2022) have used photonic crystal fiber sensor combined with chitosan-polyvinyl alcohol and glutathione functionalized gold nanoparticles to measure the Pb^{2+} solution [24]. Kumar et al. (2022) have used a interferometer fiber sensor composed of fiber Bragg grating and AuNPs-maleic acid sensitive film to measure the Pb^{2+} concentration [5]. Li et al. (2022) have used the smart hydrogel-based tapered microfiber sensor to detect Pb^{2+} concentration in water [25]. However, the above sensors are either very expensive and complex to manufacture or have low sensitivity. Fiber grating fabrication requires expensive CO_2 lasers, excimer UV lasers or femtosecond lasers [26–28], and microfiber coil resonators are extremely difficult to fabricate. The fabrication of photonic crystal fibers is even more troublesome, usually requiring ultrasonic perforation [29], chemical etching [30], and extrusion methods [31] that require difficult operations, some of which require the use of expensive instruments and harmful chemicals. Surface plasmon resonance of optical fibers requires precious metal particles and complex interlayer structures [32]. To solve these problems, the conical microfiber interferometer is widely used for concentration analysis due to its superior swift field, simple fabrication, low cost, and ultra-high sensitivity [33]. The sensing performance of the interferometer can be further improved by coating special polymer films on the fiber surface [34,35].

As an emerging material, dopamine (DA) can be directly self-polymerized on the surface of various materials to form a viscous polydopamine (PDA) film-coating. The large number of reactive groups in PDA such as catechol and amino groups can provide multiple binding sites, allowing PDA to be used as a chemical cross-linking layer for secondary surface modification reactions [36]. Because of these advantages, as a multifunctional material, PDA coating has been widely used in many fields such as catalysis, molecular immobilization and electrochemical biosensing [37]. PDA can be formed by two different pathways: covalent polymerization and non-covalent self-assembly [38]. Based on the polymerization mechanism, there are catechol or hydroquinone functional groups, indole groups, amino groups, imino groups and indole / catechol P-systems in PDA, thus PDA has good adhesion to all types of substrates [36]. The existence of these groups in PDA also offers the opportunity of further coupling functional groups of interest. Maleic acid (MA) is selected as a suitable intermediate material which contains two carboxyl groups [39], and due to the carboxyl group action, MA can not only form amide bonds with PDA [40] but also attract Pb^{2+} in aqueous solutions [39], that provides practical value for subsequent microfiber sensors to detect Pb^{2+} concentration. Therefore, the structure combining PDA-MA thin film with microfiber interferometer structure is submitted to further optimize the sensing properties (simplicity, sensitivity and specificity).

In this paper, a microfiber interferometer sensor based on functional

sensitive film (PDA-MA (PDA, polydopamine; MA, maleic acid)) for detecting lead ion concentration is proposed and demonstrated. The PDA-MA functionalized sensitive film in-situ on the microfiber surface, which is grown by a one-step dip coating method. Due to the unique tapered structure and ultra-fine diameter of this interferometer, it offers excellent sensing performance, including a RI sensitivity response of 1243.455 nm/RIU and a low temperature cross-response of −0.04 nm/°C. Subsequent experimental analysis shows that Pb^{2+} is significantly detected in the concentration range of 10^{-14}-10^{-6} mol/L, and its sensitivity is up to 1.85 × 10^{8} nm/(mol/L) in the range of 10^{-14}-10^{-10} mol/L with a detection limit of 0.1678 ppb. At the same time, the sensor also has excellent stability and unique specificity for lead ions.

2. Experimental Section

2.1. Regents and instruments

Dopamine hydrochloride (DA) (98%), maleic acid (MA) (AR, ≥99%, HPLC), lead chloride ($PbCl_2$) (AR, 99.5%), nickel chloride hexahydrate ($NiCl_2{\cdot}6H_2O$) (AR, 99%), sodium chloride (NaCl) (99.5%) and mercury nitrate monohydrate ($HgN_2O_6{\cdot}H_2O$) (AR) were purchased from Shanghai Macklin Biochemical Technology Co., Ltd. Tris-Hydrochloride Buffer (Tris-HCl) (1 mol, pH 8.5) and cadmium nitrate tetrahydrate ($CdN_2O_6{\cdot}4H_2O$) (AR, 99%) were bought from Aladdin Chemistry, Co., Ltd. Deionized water (DI) was used throughout all experiments.

The optical laboratory devices included an amplified spontaneous emission (ASE) light source, optical spectrum analyzer (OSA, Anritsu MS9740A, Japan), optical fiber fusion splicer (Fujikura FSM-60S, Japan) and digital refractometry (Reichert 13940000, USA). The sample film characterization was tested by Fourier Transform Infrared Spectrometer (FTIR, Thermo Scientific is50, USA). The morphology of microfiber surface was characterized by scanning electron microscopy (SEM, Zeiss Sigma HD, Germany), and the energy dispersive spectrometer (EDS, Zeiss Sigma HD, Germany) spectroscopy was analyzed the elements of PDA-MA-Pb^{2+} on the surface of the fabricated sensor. The macroscopic structure of microfibers was observed using metallurgical microscopy (Caikon DMM-200C, China). The notch mold used for the experiment was made by 3D printer (DDKUN D160max, China). The position operation of microfiber fabricating process was used by a motion controller (Zolix, MC600, China).

2.2. Experimental setup

As shown in Fig. 1(a, top), the light was emitted from the ASE light source (1528–1603 nm) with the output power of 10 dBm, and passed through the microfiber sensor, finally collected by the OSA (600–1700 nm) with a resolution of 0.03 nm to record the interference spectrum. The microfiber sensor was placed inside a custom 3D printed cross-shaped mold to protect the optic fiber and facilitate dripping and storage of the solution, as shown in Fig. 1 (a, bottom). The mold had three recesses. The middle of a mold had a deeper depth, which was designed to ensure that the microfiber section was partially placed in this groove and could be fully immersed in the solution. This part had a depth of 2 mm, a width of 5 mm and a length of 5 cm. The grooves on both sides had the same depth and specifications with a depth of 1 mm, a width of 2 mm and a length of 1.5 cm, which were used to hold the fiber. In order to fix the mold on the platform better, the outside of the mold was made to be beveled.

2.3. Sensor fabrication

The tapered microfiber was fabricated by heating and uniformly stretching the commercial fiber. The fiber diameter was gradually reduced from 125 μm to several tens of micrometers by heating the fiber for 6 s with a butane flame gun and then automatically and uniformly stretching the fiber with a motion controller. A stable microfiber interferometer was successfully fabricated. In Fig. 1(a, bottom), the schematic of the fabricated microfiber structure included of two 3 mm conical transition areas and a uniform area with a length of 12 mm and a diameter of 10 μm. The microfiber interferometer was then completely immersed in the prepared PDA-MA mixed solution at room temperature for 90 min.

The PDA-MA mixed solution was prepared as follows. Weigh 10 mg of DA into 5 mL of Tris-HCl to prepare the 2 g/L concentration of DA solution [37], and then stir the above solution for 30 min at normal temperature and pressure to obtain a brown PDA solution. MA (2.5 mL, 10 mM) was added to the prepared PDA solution and stirred for 30 min at normal temperature and pressure. Self-assembly binding of carboxyl group of MA to the amino group of PDA surface occurred [40].

3. Results and discussion

3.1. Sensing principle and mechanism

Due to the thinning of the fiber diameter in the middle area of the microfiber sensor, both the core and the cladding diameter of the fiber are reduced, resulting in a mismatch, so that when the incident light enters to the microfiber, it results in a portion of the light will continue to propagate along the core and the other part will enter the conical transition area of the fiber to propagate and excite the higher-order modes [41]. The core and cladding modes are transmitted simultaneously with the mainly propagating fundamental mode (HE_{11}) and higher-order mode (HE_{12}) [41]. When light is transmitted to the other end of the tapered fiber, the HE_{11} mode and the HE_{12} mode are coupled [42]. Due to the different effective refractive indices of the core and cladding modes, this constitutes a Mach-Zehnder interferometer that outputs a stable distribution of the transmission spectrum [43].

According to the optical interference principle, the output intensity $\boldsymbol{I}$ of the MZI structure can be expressed as [44]:

$$\boldsymbol{I} = \boldsymbol{I}_{core} + \boldsymbol{I}_{cladding} + 2\sqrt{\boldsymbol{I}_{core}\boldsymbol{I}_{cladding}}\cos\boldsymbol{\theta} \tag{1}$$

where $\boldsymbol{I}_{core}$ and $\boldsymbol{I}_{cladding}$ represent the optical intensity of the core and cladding modes in the fiber, respectively. $\boldsymbol{\theta}$ represents the total phase difference between the core and cladding modes in the fiber, which is influenced by the change of effective refractive index. According to the transmission principle of light in optical fiber, it can be deduced that $\boldsymbol{\theta}$ approximate expression as [43,44]:

$$\boldsymbol{\theta} = \left(\frac{2\pi \boldsymbol{L}\Delta \boldsymbol{n}_{eff}}{\lambda}\right) \tag{2}$$

where $\boldsymbol{L}$ is the length of the tapered area, which is the effective length of the dual-mode interference path, and the optical range difference between the two modes is almost the same, and λ is the wavelength of the propagating light in the fiber. $\Delta \boldsymbol{n}_{eff}$ is the effective refractive index difference between the cladding and the core [44], which can be expressed as:

$$\Delta \boldsymbol{n}_{eff} = \boldsymbol{n}_{eff}^{cladding} - \boldsymbol{n}_{eff}^{core} \tag{3}$$

where $\boldsymbol{n}_{eff}^{cladding}$ is the effective refractive index of the cladding and $\boldsymbol{n}_{eff}^{core}$ is the effective refractive index of the core. When the phase difference $\boldsymbol{\theta} = (2\boldsymbol{n}+1)\boldsymbol{\pi}$, the Mach-Zehnder interference condition is satisfied, and the resonant peak wavelength (corresponding to the trough) of the transmission spectrum can be introduced by Formula. (4) [44]:

$$\lambda_n = \frac{2\Delta \boldsymbol{n}_{eff}\boldsymbol{L}}{2\boldsymbol{n}+1} \tag{4}$$

where λ_n represents the wavelength of the $\boldsymbol{n}_{th}$ order resonance peak. The effective refractive index difference $\Delta \boldsymbol{n}_{eff}$ change can cause the wavelength λ_n shift.

In general, the external RI sensitivity of an interferometer can be

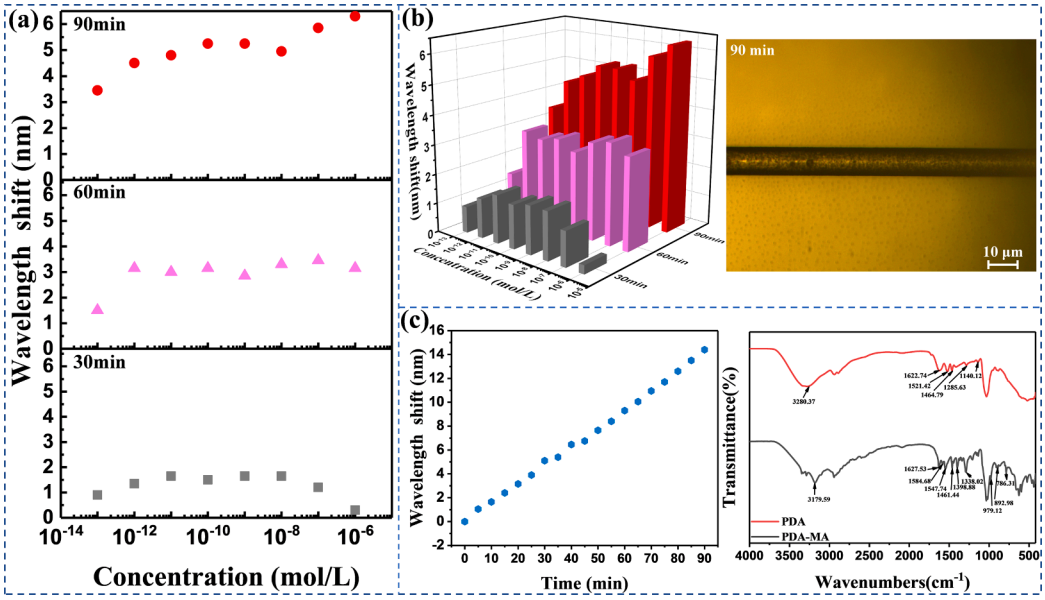

Fig. 2. (a) The detecting response of lead ion under different PDA-MA immersing times with the functional sensing probe; (b) A summarized histogram (left); the metallographic microscopic image after immersing 90 min (right); (c) The wavelength shift of the interference spectrum preparing the functional sensing probe in 90 min (left); the Fourier Transform Infrared Spectroscopy of PDA and PDA-MA film (right).

expressed by [33,41,45]:

$$\frac{d\lambda}{dn_{ext}} = \lambda_n \frac{1}{\Gamma}\left(\frac{1}{\Delta n_{eff}} \frac{d\Delta n_{eff}}{dn_{ext}}\right) \tag{5}$$

where $\Gamma = 1 - \frac{\lambda_n}{\Delta n_{eff}} \frac{d\Delta n_{eff}}{d\lambda}$ is the dispersion coefficient, which is a negative number [41], and n_{ext} is the RI of the surrounding medium. $\frac{d\Delta n_{eff}}{dn_{ext}}$ is the index dependent change caused by small changes in RI of the external environment [45]. When the external RI increases, the effective exponents of both fundamental and higher-order modes rise correspondingly [46]. It is the exponential difference due to the tiny diameter of the microfiber that leads to its high RI sensitivity.

When a functional film is attached to the surface of the microfiber, it constitutes a microfiber sensing probe that can detect specific substances, as shown in Fig. 1 (b). Functional groups such as amino, carboxyl and hydroxyl groups are often used in heavy metal ion detection because they have been shown to have effective binding sites with heavy metal ions [24,39]. Usually, MA has a large number of carboxyl groups [39]. In detail, MA has the general formula HOCCH = $CHCO_2H$, wherein it has two carboxyl groups, one of which is attached to the polydopamine by dehydration condensation with the amino group in the polydopamine to form an amide bond [40]. The second carboxyl group of MA trapped Pb^{2+} as a way to change the RI (n_{PDA-MA}) of the lead ion-sensitive film, which can cause red-shift the wavelength. The RI sensitivity of microfiber ion-sensor derived from Formula (5) is demonstrated as:

$$\frac{d\lambda}{dn_{PDA-MA}} = \lambda_n \frac{1}{\Gamma}\left(\frac{1}{\Delta n_{eff}} \frac{d\Delta n_{eff}}{dn_{PDA-MA}}\right) \tag{6}$$

When the PDA-MA coated microfiber sensing probe is exposed to Pb^{2+} concentration, the spectrum shifts toward long-waves indicating successful ion-detection.

3.2. Refractive index and temperature performance

Fig. 1 (c, left) shows the spectrum of the microfiber interferometer with detecting wavelength marked in red dot. In order to accurately measure the sensing performance of microfiber interferometer to external RI changes, the sodium chloride solutions as the simulated external RI solution are used by the digital refractometer to determine RI values. The redshift spectrums of different RI solutions are recorded at room temperature (26℃). In Fig. 1 (c, right), the experiment results shows that the RI sensitivity of this interferometer reaches 1243.455 nm/RIU in the range of 1.3342 ~ 1.3511 with a fitting degree R^2 of 0.99279.

In addition, the temperature analysis is performed for the range from 30 to 80℃. The interferometer is placed in a thermostat and the spectrum is recorded every 10 °C. In order to ensure the uniform heating to minimize experimental errors, it is very important that before storing the spectral data, the temperature needs to keep 5 min for reaching the preset value. In Fig. 1 (c right, inset), the wavelength of the transmission spectrum tends to blue-shift as the ambient temperature increases, and the linear fit shows a low temperature sensitivity of −0.04 nm/°C with a fit R^2 of 0.99611, which indicates that the microfiber interferometer has a low temperature cross-sensitivity.

3.3. Characterization of the functional sensing probe

The combination of nano-functional layer with microfiber interferometer under specific conditions is of paramount importance to obtain the functional sensing probe. A functional layer consisting of a PDA-MA mixed solution (Section 2.3 for preparation method) is uniformly applied to the microfiber surface by a one-step dip-drop coating method. To determine the optimal time of the functional film, the similar structure of microfiber interferometer is soaked in PDA-MA solution for 30, 60 and 90 min to prepare the recognition sensing probe for detecting lead ions. The wavelength responses of these probes in three coating times for the same concentration gradient (10^{-13}, 10^{-12}, 10^{-11}, 10^{-10}, 10^{-9}, 10^{-8}, 10^{-7} and 10^{-6} mol/L) are shown in Fig. 2 (a). It can be intuitively that when the coating time is 90 min, the detecting different concentrations of lead ion is best, and the wavelength shift increases significantly, which has a red-shift trend with the overall wavelength shift reaching 6.3 nm. As a contrastive study, when the coating time is 30 or 60 min, the detection effect of lead ion is a flat shift trend and a small amount of redshift. Fig. 2 (b, left) shows the statistical histogram of wavelength shift for the recognition sensor at three coating times for detecting lead ions. Thus, the optimal time for the functional sensing probe is 90 min. Fig. 2 (b, right) shows the microscope image of the functional sensing probe (90 min). In detail, there are obvious black

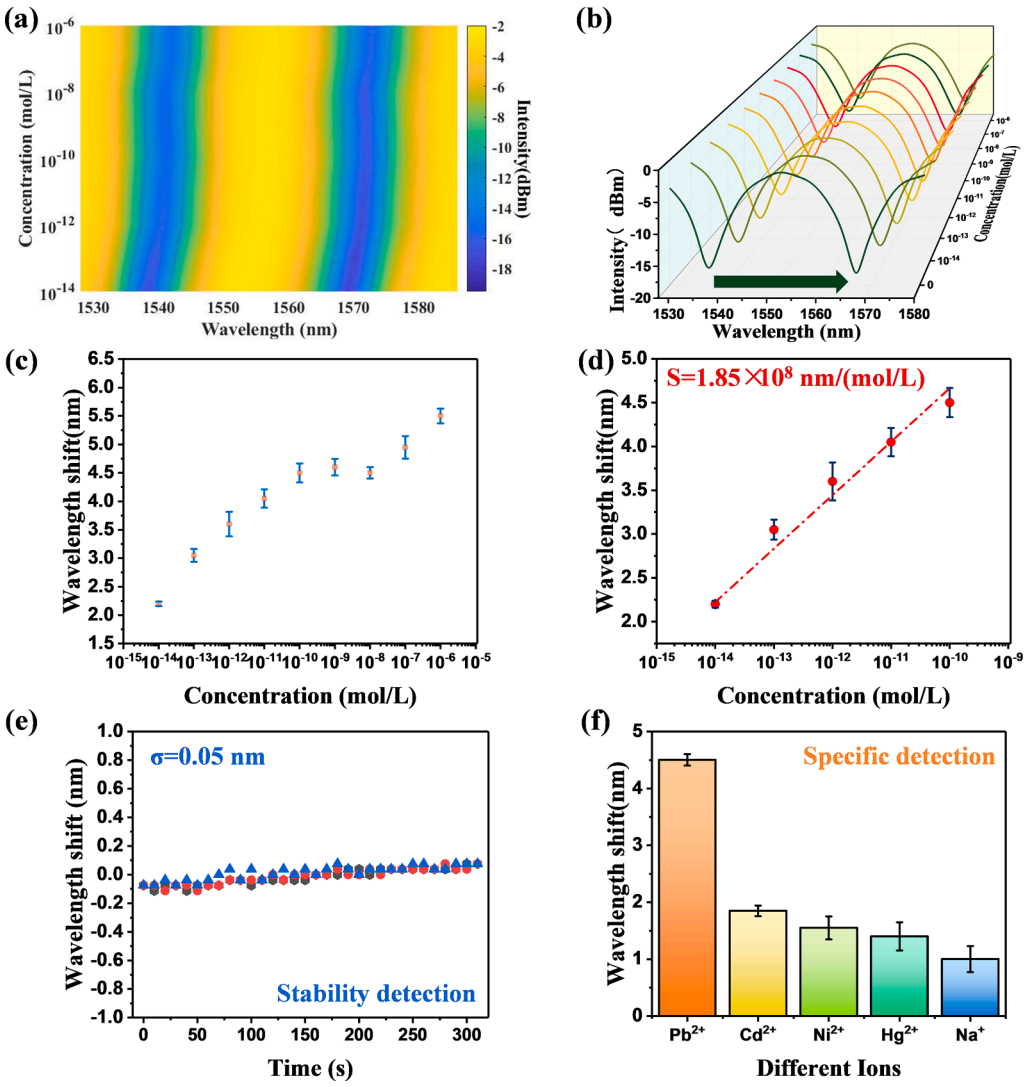

Fig. 3. (a) The wavelength response of the interference spectrum for using PDA-MA film functional sensing probe to detect Pb^{2+} concentration. (b) The shift of the corresponding interference spectrum. (c) The response of the sensing probe to Pb^{2+} in the range of 10^{-14}-10^{-6} mol/L. (d) The linear response of the probe to Pb^{2+} in the low range of 10^{-14}-10^{-10}mol/L. (e) The wavelength shift by recording the spectrum of functional sensing probe in three times of deionized water. (f) Response of the sensing probe to different heavy metal ions.

areas on the fiber surface appearing many uniform and fine particles. Fig. 2 (c, left) shows the change of wavelength spectrum in 90 min. As the coating time increases, the wavelength gradually redshifts with the even growth trend. The final amount of red shift reaches 14.4 nm with the rate of 0.16 nm/min.

To verify that the MA has been successfully connected to the PDA, the FTIR spectrum in Fig. 2 (c, right) shows the two samples (PDA film and PDA-MA film). The red line in the figure shows the infrared spectrum of PDA, where the absorption peak around 3280.37 cm^{-1} is the stretching vibration of the N–H group of catechol. The characteristic peak is 1622.74 cm^{-1} due to the stretching vibration of the aromatic ring and the bending vibration of the N–H bond. The characteristic peak of 1521.42 cm^{-1} corresponds to the shearing vibration of the N–H bond. The absorption peaks at 1464.79 cm^{-1} peak is related to the skeleton vibration of benzene. The absorption peak of 1285.63 cm^{-1} and 1140.12 cm^{-1} can be attributed to the C-O stretching and primary amine vibration of PDA [47,48]. The infrared spectrum of PDA combined with MA is shown as the black line in Fig. 2 (c, right), and the vibration peak at 3280.37 cm^{-1} in PDA is attenuated to 3179.59 cm-1, which can be presumed that the amino part is involved in the reaction [40]. The absorption peak at 1627.53 cm^{-1} corresponds to the C = O bond in maleic acid. 1547.74 cm^{-1}, 1584.68 cm^{-1} and 1461.44 cm^{-1} correspond to C=C bond in maleic acid, 1398.88 cm^{-1} and 1338.02 cm^{-1} correspond to –OH in maleic acid. The absorption peaks of 979.12 cm^{-1}, 892.98 cm^{-1}, and 786.31 cm^{-1} correspond to the = C–H bond in maleic acid [49,50]. The above phenomena indicate that the PDA-MA synthesis of functional membrane is successful.

3.4. Pb^{2+} detection and specific detection

The schematic diagram of the PDA-MA thin-film functionalized microfiber sensing probe for the detection of Pb^{2+} concentration is shown in Fig. 1(b). According to Section 2.3, a layer of PDA-MA functional film is grown on the fiber surface by in situ one-step immersion method, which is successfully fabricated a good probe. This probe detects Pb^{2+} solutions in the order from low to high concentrations, and the corresponding interference spectrums are recorded for each concentration. Pb^{2+} solutions with different concentrations of 10^{-14}, 10^{-13}, 10^{-12}, 10^{-11}, 10^{-10}, 10^{-9}, 10^{-8}, 10^{-7} and 10^{-6} mol/L are obtained by dissolving $PbCl_2$ powder with DI. The carboxyl group of MA can trap Pb^{2+} in aqueous solution [39], which affects the RI of the functional film of the microfiber interferometer resulting the wavelength change of the interference spectrum.

Fig. 3 (a) and Fig. 3 (b) shows the detection result for Pb^{2+} concentrations. The blue region in Fig. 3 (a) represents the wavelength shift with increasing Pb^{2+} concentration, which indicates an obvious redshift phenomenon in the interference spectrum. Fig. 3 (b) shows the macroscopic shift of the corresponding interference spectra, and it is clear that the interference spectra drift in the direction of longer wavelengths. Through three experiments under the same steps and conditions, the

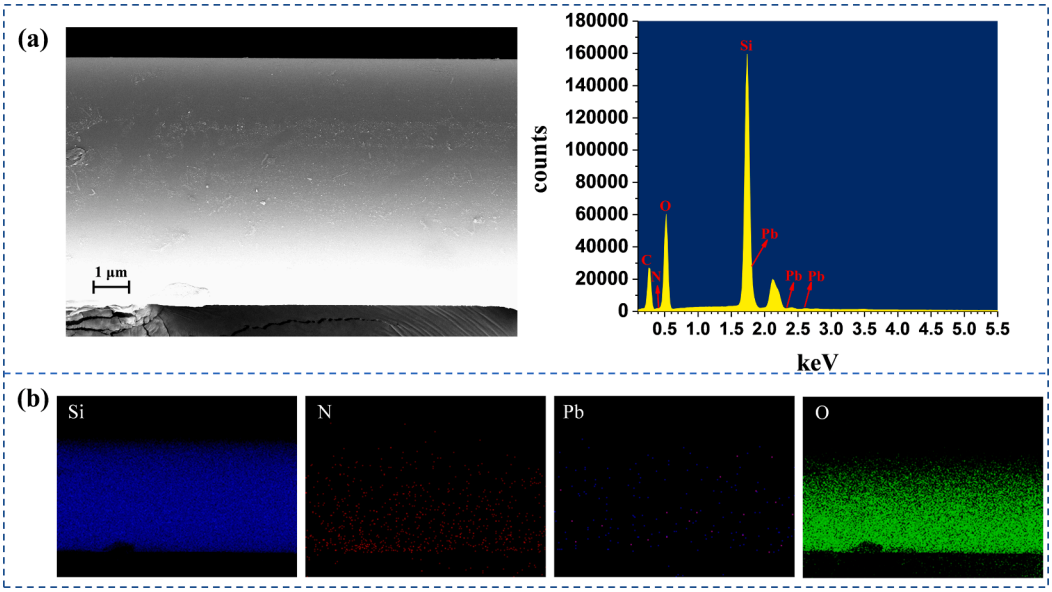

Fig. 4. (a) SEM characterization of the fiber coated with PDA-MA film (left); EDS analysis (right) with the mapping analysis (b) of the sensing probe surface after detecting Pb^{2+}.

obtained wavelength shift trend with error analysis (Relative Standard Deviation) is shown in Fig. 3 (c). It can be seen that the detection curve gradually saturates greater than 10^{-10} mol/L. The main reason for this phenomenon is the film limited surface area on fiber. Fig. 3 (d) shows in detail the response of the functionalized microfiber sensing probe to Pb^{2+} concentration in the ultra-low range of 10^{-14}-10^{-10} mol/L with a detection sensitivity of 1.85×10^{8} nm/(mol/L). The wavelength shift within the error range of this PDA-MA film functional probe is obtained by recording the spectrum in DI for three experiments by the same steps and conditions to verify the stability, as shown in Fig. 3 (e). In detail, the average wavelength shift deviation of the three experiments is 0.15 nm and the average standard deviation is 0.05 nm, which is a small value within the acceptable range and the main reason for the error is caused by thermal noise. The theoretical detection limit can be calculated as $\boldsymbol{LOD} = 3\boldsymbol{\sigma}/\boldsymbol{S}$, where $\boldsymbol{\sigma}$ is the standard deviation of the error measurement, which has been obtained as 0.05 nm, and $\boldsymbol{S}$ is the slope of the calibration curve [51], which is 1.85×10^{8} nm/(mol/L). The $\boldsymbol{LOD}$ can be calculated as 0.81×10^{-9} mol/L (0.1678 ppb), which is lower than the concentration of lead ions in drinking water stipulated by WHO (10 ppb). Combining all the above analysis and test results, it can be concluded that the PDA-MA functionalized microfiber sensor has high accuracy, good repeatability and superior stability in response to Pb^{2+}.

To verify the specificity of the sensor, three experiments are performed with the same method for different heavy metal ions (Cd^{2+}, Ni^{2+}, Hg^{2+}, Na^{+}) with concentrations in the range of 10^{-14}-10^{-10} mol/L. As shown in Fig. 3 (f), the wavelength shifts of the different heavy metal ions relative to DI resulted in 4.5 nm (Pb^{2+}), 1.85 nm (Cd^{2+}), 1.55 nm (Ni^{2+}), 1.4 nm (Hg^{2+}), and 1 nm (Na^{+}). It can be seen from the figure that the response of the sensor to Pb^{2+} is significantly higher than that of other heavy metal ions because the functional membrane with carboxyl groups exerts a more obvious force on lead ions, indicating that the sensor has good specificity for lead ions.

3.5. Characterization of the functional sensing probe with Pb^{2+}

The surface morphology and chemical composition of the PDA-MA functionalized probe after capturing Pb^{2+} are analyzed by SEM and EDS, as shown in Fig. 4. SEM image of the fiber with functional layer

Table 1
Comparison of different optic fiber sensors for Pb^{2+} detection.

Structure	Functional Materials	Concentration range	LOD	Sensitivity	Cost	Manufacturing difficulty	Refs.
Clad etched- fiber Bragg grating	AuNPs-maleic acid	10^{-14}-10^{-7} mol/L (2×10^{-7}-20.72 ppb)	10^{-14} mol/L (2×10^{-7} ppb)	0.56 nm/(mol/L) (2.703×10^{-9} nm/ppb)	High	difficultly	[3]
Microfiber coil resonator	Black phosphorus	0.1–5 × 10^{4} ppb	0.0285 ppb	—	Medium	Medium	[5]
Long Period Fiber Grating	Periodic mesoporous organosilica	0.093–96 ppm (93–9.6 × 10^{4} ppb)	20 ppb	1 nm/100 ppb (0.01 nm/ppb)	High	difficultly	[16]
Tilted Fiber Grating	Black phosphorus	0.1–1.5 × 10^{7} ppb	0.25 ppb	0.5 × 10^{-3} dB/ppb	High	Medium	[17]
Microfiber with two fiber Bragg gratings	L-glutathione	5–50 μg/L (5–50 ppb)	5 μg/L (5 ppb)	—	Medium	difficultly	[18]
Single mode fiber-photonic crystal fiber	Chitosan-polyvinyl alcohol, glutathione-AuNPs	1–50 ppb	1.6 ppb	0.031 nm/ppb	High	difficultly	[19]
No-core fiber/Few-mode fiber/ No-core fiber	Smart hydrogel	2×10^{-7}-1.2×10^{-6} mol/L (41.44–248.64 ppb)	2.452×10^{-8} mol/L (5.0805 ppb)	8.155×10^{5} nm/(mol/L) (3.936×10^{-3} nm/ppb)	High	difficultly	[20]
Tapered microfiber interferometer	Polydopamine- maleic acid	10^{-14}-10^{-6} mol/L (2×10^{-7}-207.2 ppb)	0.81×10^{-9} mol/L (0.1678 ppb)	1.85×10^{8} nm/(mol/L) (0.893 nm/ppb)	Low	Easy	This work

shows a uniform and dense nanoparticle film on the surface in Fig. 4 (a, left). Fig. 4 (a, right) shows the results of the elemental analysis of the fiber surface. The presence of N element indicates the successful attachment of the PDA-MA functional layer [52] and the presence of Pb element proves that the functionalized fiber can successfully trap Pb^{2+}. Fig. 4 (b) shows the corresponding mapping analysis of Si, N, Pb and O elements, which further verifies that the PDA-MA functional film is successfully wrapped on the fiber surface and can be used to detect lead ions in aqueous solutions.

To facilitate comparison, Table 1 shows the comparison between this sensor and other methods that use optical fiber to detect the concentration of Pb^{2+}. It can be clearly seen that the functionalized microfiber sensor not only can accurately detect Pb^{2+} concentrations in the ultra-low concentration range with extremely high sensitivity and very low LOD, but also is easy to manufacture and inexpensive compared with some currently popular methods that use optical fibers to detect Pb^{2+} concentrations. All these fully demonstrate the advantages of the PDA-MA functionalized microfiber sensor for trace Pb^{2+} achieved by one-step synthesis method.

4. Conclusion

In this work, a PDA-MA thin film functionalized microfiber interferometer with high stability and good selectivity is proposed for detecting lead ions. The microfiber interferometer has a high RI sensitivity response of 1243.455 nm/RIU and a low temperature cross-response of −0.04 nm/℃. Functional film is in-situ grown on the surface of microfiber interferometer by one-step immersion method. Experimental results demonstrate that the sensor has obvious response to Pb^{2+} in the detection concentration range of 10^{-14}-10^{-6} mol/L and a sensitivity of 1.85×10^{8} nm/(mol/L) in the ultra-low range of 10^{-14}-10^{-10} mol/L with a detection limit of 0.1678 ppb. By using the repeated measurements of other common metal ions, it is verified that this proposed sensor has superior stability and specificity. The detection concentration of the sensor is lower than the standard set by the World Health Organization, so the sensor can meet the detection of Pb^{2+} concentration in most environments. The realization of this sensor broadens the application field of optical sensors and has guiding significance for the research of optical environmental pollution sensors.

Declaration of Competing Interest

The authors declare that they have no known competing financial interests or personal relationships that could have appeared to influence the work reported in this paper.

Acknowledgments

This work was supported by National Natural Science Foundation of China (62005147, 62175055, 62175054); International Cooperation and Exchange of the National Natural Science Foundation of China (62020106014); Natural Science Foundation of Hebei Province (F2021109003), Science and Technology Research Project of Higher Education of Hebei Province (BJ2021093); Hebei key Laboratory of Optical Fiber Biosensing and Communication Devices (SZX2022010).

References

[1] Y. Wang, G. Zhu, M.Y. Li, R. Singh, C. Marques, R. Min, S. Kumar, Water pollutants p-Cresol detection based on Au-ZnO nanoparticles modified tapered optical fiber, IEEE T. Nanobiosci. 20 (2021) 377–384, https://doi.org/10.1109/TNB.2021.3082856.

[2] M.Y. Li, R. Singh, C. Marques, B.Y. Zhang, S. Kumar, 2D material assisted SMF-MCF-MMF-SMF based LSPR sensor for creatinine detection, Opt. Express 29 (2021) 38150–38167, https://doi.org/10.1364/OE.445555.

[3] W.Q. Lai, Y.F. Chang, F.N. Chou, D.M. Yang, Portable FRET-based biosensor device for on-site lead detection, Biosensors 12 (2022) 17, https://doi.org/10.3390/bios12030157.

[4] Z.L.L. He, X.E. Yang, P.J. Stoffella, Trace elements in agroecosystems and impacts on the environment, J. Trace Elem. Med. Biol. 19 (2005) 125–140, https://doi.org/10.1016/j.jtemb.2005.02.010.

[5] N.V. Kumar, B.S. Kavitha, S. Asokan, Selective detection of lead in water using etched fiber Bragg grating sensor, Sens. Actuators B-Chem. 354 (2022) 7, https://doi.org/10.1016/j.snb.2021.131208.

[6] S.V. Dimitrova, Use of granular slag columns for lead removal, Water Res. 36 (2002) 4001–4008, https://doi.org/10.1016/S0043-1354(02)00120-3.

[7] Y. Yin, S. Li, S.B. Wang, S.J. Jia, J. Ren, G. Farrell, E. Lewis, P.F. Wang, Ultra-high-resolution detection of Pb^{2+} ions using a black phosphorus functionalized microfiber coil resonator, Photonics Res. 7 (2019) 622–629, https://doi.org/10.1364/prj.7.000622.

[8] M. Ali, Preconcentration and determination of trace amounts of heavy metals in water samples using membrane disk and flame atomic absorption spectrometry, Chin. J. Chem. 25 (2007) 640–644, https://doi.org/10.1002/cjoc.200790119.

[9] R.Q. Zhou, B.J. Li, N.J. Wu, G. Gao, J.S. You, J.B. Lan, Cyclen-functionalized perylenebisimides as sensitive and selective fluorescent sensors for Pb^{2+} in aqueous solution, Chem. Commun. 47 (2011) 6668–6670, https://doi.org/10.1039/c1cc11200g.

[10] A.U. Alam, M.M.R. Howlader, N.-X. Hu, M.J. Deen, Electrochemical sensing of lead in drinking water using β-cyclodextrin-modified MWCNTs, Sens. Actuat. B-Chem. 296 (2019), https://doi.org/10.1016/j.snb.2019.126632.

[11] R. Sitko, P. Janik, B. Zawisza, E. Talik, E. Margui, I. Queralt, Green approach for ultratrace determination of divalent metal ions and arsenic species using total-reflection X-ray fluorescence spectrometry and mercapto-modified graphene oxide nanosheets as a novel adsorbent, Anal. Chem. 87 (2015) 3535–3542, https://doi.org/10.1021/acs.analchem.5b00283.

[12] F. Chai, C.A. Wang, T.T. Wang, L. Li, Z.M. Su, Colorimetric detection of Pb^{2+} using glutathione functionalized gold nanoparticles, ACS Appl. Mater. Inter. 2 (2010) 1466–1470, https://doi.org/10.1021/am100107k.

[13] L.L. Liu, S.P. Morgan, R. Correia, S. Korposh, A single-film fiber optical sensor for simultaneous measurement of carbon dioxide and relative humidity, Opt. Laser Technol. 147 (2022) 9, https://doi.org/10.1016/j.optlastec.2021.107696.

[14] Y. Ran, J.Q. Long, Z.Y. Xu, Y. Yin, D.L. Hu, X.T. Long, B.O. Guan, Harmonic optical microfiber Bragg grating immunosensor for the accelerative test of cardiac biomarker (cTn-I), Biosens. Bioelectron. 179 (2021), 113081, https://doi.org/10.1016/J.BIOS.2021.113081.

[15] D.Q. Yang, Y.G. Liu, Y.X. Wang, T. Zhang, M. Shao, D.K. Yu, H.W. Fu, Z.N. Jia, Integrated optic-fiber sensor based on enclosed EFPI and structural phase-shift for discriminating measurement of temperature, pressure and RI, Opt. Laser Technol. 126 (2020) 7, https://doi.org/10.1016/j.optlastec.2020.106112.

[16] M. Zhang, X. Ma, L. Wang, S. Lai, H. Zhou, H. Zhao, Y. Liao, Progress of optical fiber sensors and its application in harsh environment, Photonic Sens. 1 (2011), https://doi.org/10.1007/s13320-010-0012-1.

[17] Y. Cao, X.D. Wang, T. Guo, Y. Ran, X.H. Feng, B.O. Guan, J.P. Yao, High-resolution and temperature-compensational HER_2 antigen detection based on microwave photonic interrogation, Sens. Actuators B-Chem. 245 (2017) 583–589, https://doi.org/10.1016/j.snb.2017.01.085.

[18] P. Xiao, Z.Y. Xu, D.M. Hu, L.L. Liang, L.P. Sun, J. Li, Y. Ran, B.O. Guan, Efficiently writing bragg grating in high-birefringence elliptical microfiber for label-free immunosensing with temperature compensation, Adv. Fiber Mater. 3 (2021) 321–330, https://doi.org/10.1007/s42765-021-00087-7.

[19] Y. Ran, Z.Y. Xu, M.F. Chen, W. Wang, Y. Wu, J.X. Cai, B.O. Guan, Fiber-optic theranostics (FOT): interstitial fiber-optic needles for cancer sensing and therapy, Adv. Sci. 9 (2022) 2200456, https://doi.org/10.1002/ADVS.202200456.

[20] R. Raghunandhan, L.H. Chen, H.Y. Long, L.L. Leam, P.L. So, X. Ning, C.C. Chan, Chitosan/PAA based fiber-optic interferometric sensor for heavy metal ions detection, Sens. Actuators B-Chem. 233 (2016) 31–38, https://doi.org/10.1016/j.snb.2016.04.020.

[21] J. Du, J. Cipot-Wechsler, J.M. Lobez, H.P. Loock, C.M. Crudden, Periodic mesoporous organosilica films: key components of fiber-optic-based heavy-metal sensors, Small 6 (2010) 1168–1172, https://doi.org/10.1002/smll.201000269.

[22] C. Liu, Z. Sun, L. Zhang, J. Lv, X.F. Yu, L. Zhang, X. Chen, Black phosphorus integrated tilted fiber grating for ultrasensitive heavy metal sensing, Sens. Actuat. B-Chem. 257 (2018) 1093–1098, https://doi.org/10.1016/j.snb.2017.11.022.

[23] S.H.K. Yap, Y.H. Chien, R. Tan, A.R.B. Alauddin, W.B. Ji, S.C. Tjin, K.T. Yong, An advanced hand-held microfiber-based sensor for ultrasensitive lead ion detection, ACS Sens. 3 (2018) 2506–2512, https://doi.org/10.1021/acssensors.8b01031.

[24] A. Al Noman, J.N. Dash, X. Cheng, H.Y. Tam, C.Y. Yu, PCF based modal interferometer for lead ion detection, Opt. Express 30 (2022) 4895–4904, https://doi.org/10.1364/oe.447272.

[25] G.S. Li, Z. Liu, J.X. Feng, G.Y. Zhou, X.G. Huang, Pb^{2+} fiber optic sensor based on smart hydrogel coated Mach-Zehnder interferometer, Opt. Laser Technol. 145 (2022) 7, https://doi.org/10.1016/j.optlastec.2021.107453.

[26] S.H. Cai, G. Álvaro, X.J. Zhang, T. Guo, C. Caucheteur, Palladium-coated plasmonic optical fiber gratings for hydrogen detection, Opt. Lett. 44 (2019) 4483–4486, https://doi.org/10.1364/OL.44.004483.

[27] C. Zhang, C.Y. Shen, X.H. Liu, S.Y. Liu, H.C. Chen, Z.L. Huang, Z.H. Wang, T. T. Lang, C.L. Zhao, Y.M. Zhang, Pd/Au nanofilms based tilted fiber Bragg grating hydrogen sensor, Opt. Commun. 502 (2021), 127424, https://doi.org/10.1016/j.optcom.2021.127424.

[28] F. Wang, B.W. Wang, X.H. Zhang, M.D. Lu, Y. Zhang, C.S. Sun, W. Peng, High sensitivity humidity detection based on functional GO/MWCNTs hybrid nanomaterials coated titled fiber bragg grating, Nanomaterials 11 (2021) 1134, https://doi.org/10.3390/nano11051134.

[29] P. Falkenstein, C.D. Merritt, B.L. Justus, Fused preforms for the fabrication of photonic crystal fibers, Opt. Lett. 29 (2004) 1858–1860, https://doi.org/10.1364/OL.29.001858.
[30] S.J. Qiu, Y. Chen, J.L. Kou, F. Xu, Y.Q. Lu, Miniature tapered photonic crystal fiber interferometer with enhanced sensitivity by acid microdroplets etching, Appl. Optics. 50 (2011) 4328–4332, https://doi.org/10.1364/AO.50.004328.
[31] J. Rarity, J. Fulconis, J. Duligal, W. Wadsworth, P. Russel, Photonic crystal fiber source of correlated photon pairs, Opt. Express 13 (2005) 534–544, https://doi.org/10.1364/OPEX.13.000534.
[32] A. Pathak, B.D. Gupta, Palladium nanoparticles embedded PPy shell coated CNTs towards a high performance hydrazine detection through optical fiber plasmonic sensor, Sens. Actuat. B-Chem. 326 (2021), 128717, https://doi.org/10.1016/j.snb.2020.128717.
[33] W. Luo, Y. Chen, F. Xu, Recent progress in microfiber-optic sensors, Photonic Sens. 11 (2021) 45–68, https://doi.org/10.1007/s13320-021-0614-9.
[34] Y.J. Zhao, J.X. Liu, H. Li, M.J. Xu, J. Li, C.L. Jing, L.Y. Ding, Y.L. Gao, A. Zhou, An ultra-sensitive gas pressure sensor based on tapered fiber coated with PDMS film working at TAP, Opt. Laser Technol. 151 (2022) 6, https://doi.org/10.1016/j.optlastec.2022.107998.
[35] J.Y. Lu, Y. Yu, S.P. Qin, M.W. Li, Q. Bian, Y. Lu, X.Y. Hu, J.B. Yang, Z. Meng, Z. R. Zhang, High-performance temperature and pressure dual-parameter sensor based on a polymer-coated tapered optical fiber, Opt. Express 30 (2022) 9714–9726, https://doi.org/10.1364/oe.452355.
[36] S. Li, J.W. Zhang, C.S. Tan, C. Chen, C. Hu, Y.C. Bai, D. Ming, Electrochemical immunosensor based on hybrid MoS_2/Pt@Au-nanoprism/PDA for simultaneous detection of free and total prostate specific antigen in serum, Sens. Actuat. B-Chem. 357 (2022) 9, https://doi.org/10.1016/j.snb.2022.131413.
[37] G.H. Choi, D.K. Rhee, A.R. Park, M.J. Oh, S. Hong, J.J. Richardson, J.L. Guo, F. Caruso, P.J. Yoo, Ag nanoparticle/polydopamine-coated inverse opals as highly efficient catalytic membranes, ACS Appl. Mater. Inter. 8 (2016) 3250–3257, https://doi.org/10.1021/acsami.5b11021.
[38] S. Hong, Y.S. Na, S. Choi, I.T. Song, W.Y. Kim, H. Lee, Non-covalent self-assembly and covalent polymerization co-contribute to polydopamine formation, Adv. Funct. Mater. 22 (2012) 4711–4717, https://doi.org/10.1002/adfm.201201156.
[39] N. Ratnarathorn, O. Chailapakul, W. Dungchai, Highly sensitive colorimetric detection of lead using maleic acid functionalized gold nanoparticles, Talanta 132 (2015) 613–618, https://doi.org/10.1016/j.talanta.2014.10.024.
[40] M. Lubberink, W. Finnigan, C. Schnepel, C.R. Baldwin, N.J. Turner, S.L. Flitsch, One-step biocatalytic synthesis of sustainable surfactants by selective amide bond formation, Angew. Chem. Int. Edit. 61 (2022) 5, https://doi.org/10.1002/anie.202205054.
[41] Y.Y. Huang, Z. Tian, L.P. Sun, D.D. Sun, J. Li, Y. Ran, B.O. Guan, High-sensitivity DNA biosensor based on optical fiber taper interferometer coated with conjugated polymer tentacle, Opt. Express 23 (2015) 26962–26968, https://doi.org/10.1364/oe.23.026962.
[42] P.Q. Gong, X.G. Li, X. Zhou, Y.N. Zhang, N. Chen, S.K. Wang, S.Q. Zhang, Y. Zhao, Optical fiber sensors for glucose concentration measurement: a review, Opt. Laser Technol. 139 (2021) 13, https://doi.org/10.1016/j.optlastec.2021.106981.
[43] V. Ahsani, F. Ahmed, M.B.G. Jun, C. Bradley, Tapered fiber-optic mach-zehnder interferometer for ultra-high sensitivity measurement of refractive index, Sensors 19 (2019) 10, https://doi.org/10.3390/s19071652.
[44] S.H. Girei, H.N. Lim, M.Z. Ahmad, M.A. Mahdi, A.R. Zain, M.H. Yaacob, High sensitivity microfiber interferometer sensor in aqueous solution, Sensors 20 (2020) 9, https://doi.org/10.3390/s20174713.
[45] D.D. Sun, Y.M. Fu, Y.K. Yang, Label-free detection of breast cancer biomarker using silica microfiber interferometry, Opt. Commun. 463 (2020) 6, https://doi.org/10.1016/j.optcom.2020.125375.
[46] L.P. Sun, J. Li, Y.Z. Tan, S. Gao, L. Jin, B.O. Guan, Bending effect on modal interference in a fiber taper and sensitivity enhancement for refractive index measurement, Opt. Express 21 (2013) 26714–26720, https://doi.org/10.1364/oe.21.026714.
[47] Q.F. Fu, X.J. Li, Q.H. Zhang, F.Q. Yang, W.L. Wei, Z.N. Xia, A facile and versatile approach for controlling electroosmotic flow in capillary electrophoresis via mussel inspired polydopamine/polyethyleneimine co-deposition, J. Chromatogr. A 1416 (2015) 94–102, https://doi.org/10.1016/j.chroma.2015.09.014.
[48] X.S. Liu, J.M. Cao, H. Li, J.Y. Li, Q. Jin, K.F. Ren, J. Ji, Mussel-inspired polydopamine: a biocompatible and ultrastable coating for nanoparticles in vivo, ACS Nano. 7 (2013) 9384–9395, https://doi.org/10.1021/nn404117j.
[49] R. Chitra, P. Roussel, F. Capet, C. Murli, R.R. Choudhury, Molecular interactions in the anomalous salt: 2-aminopyridinium maleate maleic acid, J. Mol. Struct. 923 (2009) 45–52, https://doi.org/10.1016/j.molstruc.2009.01.057.
[50] Z. Rong, K. Qian, W.L. Cao, J. Yang, L.Y. Zeng, Z.Q. Wang, X.X. Fang, Above room temperature organic dielectric switchable and NLO Co-crystal: $C_4H_4O_4$ $_C8_{H1}9N$, Z. Anorg. Allg. Chem. 647 (2021) 764–769, https://doi.org/10.1002/zaac.202000382.
[51] L.L. Liang, L. Jin, Y. Ran, L.P. Sun, B.O. Guan, Fiber light-coupled optofluidic waveguide (FLOW) immunosensor for highly sensitive detection of p53 protein, Anal. Chem. 90 (2018) 10851–10857, https://doi.org/10.1021/acs.analchem.8b02123.
[52] M. Sureshkumar, C.K. Lee, Polydopamine coated magnetic-chitin (MCT) particles as a new matrix for enzyme immobilization, Carbohydr. Polym. 84 (2011) 775–780, https://doi.org/10.1016/j.carbpol.2010.03.036.